Takeoff Simulation of Lift + Cruise Air Taxi by Using Navier–Stokes Equations

Guru P. Guruswamy*
NASA Ames Research Center, Moffett Field, California 94035

https://doi.org/10.2514/1.J059212

Takeoff trajectory computations are made for a typical lift + cruise small transport aircraft suitable for an urban air taxi. The selected wing–body model consists of lifting and pushing propellers. Flow is modeled using the Navier–Stokes equations. A procedure is developed to embed the trajectory motion equations in an overset grid topology along with rotating blades. Results are validated with lifting line theory computations. A typical takeoff scenario is demonstrated by time-accurately integrating trajectory equations with the flow equations. The present work extends the capabilities of the current Navier–Stokes solvers to simulate trajectory motions of urban air taxi configurations.

Nomenclature

a	=	acceleration, feet/s^2
g	=	acceleration due to gravity, feet/s^2
h	=	altitude, feet
M_∞	=	freestream Mach number
m	=	mass, slugs
q	=	dynamic pressure; $0.5\rho V^2$, psi
S	=	surface area, feet^2
V	=	freestream velocity, feet/s
W	=	weight, lbs.
x, y	=	vertical and horizontal distances traveled, feet
$\dot{x}$, $\dot{y}$	=	vertical and horizontal velocities, feet/s
$\ddot{x}$, $\ddot{y}$	=	vertical and horizontal acceleration, feet/s^2
α	=	angle of attack, deg
ρ	=	air density, slugs/feet^3

I. Introduction

INNOVATIVE approaches are currently being sought for urban air taxi transportation, because flying in the open sky is potentially much faster than driving on the road. A small aircraft with electric propulsion has been identified as a commuting solution. The use of air taxis could reduce the ground traffic congestions in big cities, and the use of electric propulsion for air taxis can reduce the ever-growing demand for gasoline and the resulting pollution. NASA, with other partners, is working on a project known as Urban Air Mobility (UAM) [1]. The goal of the UAM's Grand Challenge is to provide a basis where NASA, vehicle providers, airspace technology providers, and the public can learn what achieving urban air mobility really requires. UAM demonstration of several traffic management systems for drones took place in Reno, Nevada, in 2019 [1].

Aircraft that takeoff and land vertically are already in use. The military designed vertical takeoff and land aircraft for use in locations where runways are not available [2]. For many of these vehicles, jets were used for maneuvering. A similar concept is extended for air taxis, but using electric propellers, as they are more suitable than jets for small aircraft. An electric air taxi includes lifting propellers near the wing and a pushing propeller near the rear end of the body, such as the Kitty Hawk Cora prototype, which flew for the first time in November 2017 [3]. Large companies like Boeing are teaming up together for the production of air taxis [4], and innovative configurations are rapidly evolving [5].

Received 5 November 2019; revision received 9 January 2020; accepted for publication 26 January 2020; published online 14 February 2020.

*Senior Aerospace Engineer, Computational Physics Branch. Associate Fellow AIAA.

The presence of multiple electric propellers near the wing–body of air taxis leads to complex flows. This means that accurate modeling of aerodynamic forces for understanding maneuver dynamics is crucial in the design process. To date, only linear aerodynamics are extensively used to simulate maneuver aerodynamics; however, in order to account for flow complexities—such as propeller–wing interactions, flow separations, and vortices—higher-order computational tools based on the Navier–Stokes (NS) equations are needed. Currently NS-based simulations are only addressed usually for non-maneuvering cases [6].

In this effort, a procedure to couple trajectory equations with the Reynolds-averaged Navier–Stokes (RANS) [7] equations for a takeoff scenario is presented. The procedure involves accurately modeling rigid body movements of a propeller, including blade revolutions, and trajectory motions. Flow is modeled with RANS equations using overset grids. The results are demonstrated for a typical aircraft with lifting and pushing propellers.

II. Typical Lift Cruise Air Taxi

A two-seater lift+cruise air taxi (LCAT) configuration with high lift wings, shown in Fig. 1, is generated for this work. It has the typical wing–body of a small aircraft with lifting and pushing propellers. Eight lifting propellers are aligned in front leading and backoff trailing edges on the wing. Each propeller has two blades and is placed on a pod. The pushing propeller is located near the end of the fuselage and it has three blades. The wing configuration was selected from NASA high-lift aircraft [8], and the propeller blade configurations were selected from a NACA report [9]. The blades of the lifting propeller (LPB) and pushing propellers (PPB) have aspect ratios of 5.2 and 7.2, respectively.

In this work, the RANS flow solver OVERFLOW [10] with a Spalart–Allmaras turbulence model [11] is used. OVERFLOW has the capability to model rotating rigid and flexible blades with rigid body motions. The overset grid needed for the solution contains a body-fitted near-body (NB) grid for each component and an outer-body background (BG) grid system that communicates data among NB grids. The BG grid can be either generated in OVERFLOW or provided by the user [12]. OVERFLOW generates multiple BG grids depending on a configuration suitable only for rigid body motions. In this effort, a single BG grid to accommodate all NB grids is generated separately [12] to facilitate modeling maneuvering motions.

Geometry data for both the wing–body and propeller are taken from public domain data [8,9]. The grid for this configuration is generated using the overset grid tool OVERGRID [13] and satisfying engineering grid qualities [14].

Figure 2 shows details of NB and BG grids. The wing–body contains 9 NB grids with a total of 6 million grid points. Each propeller blade and pod is modeled using 360,000 and 400,000 grid points. A single BG grid has 13 million points. The total size of the grid is 19.7 million points, which is found to be adequate to model

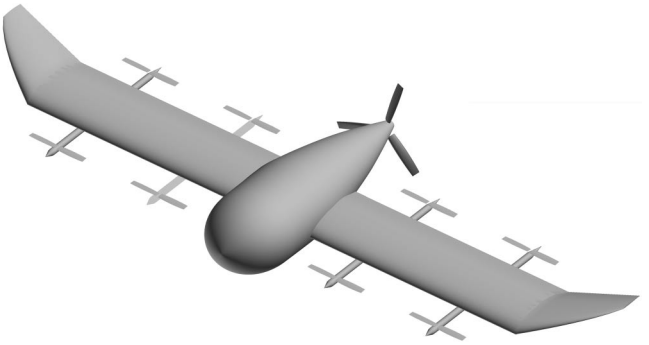

Fig. 1 A typical two-seater lift + cruise air taxi.

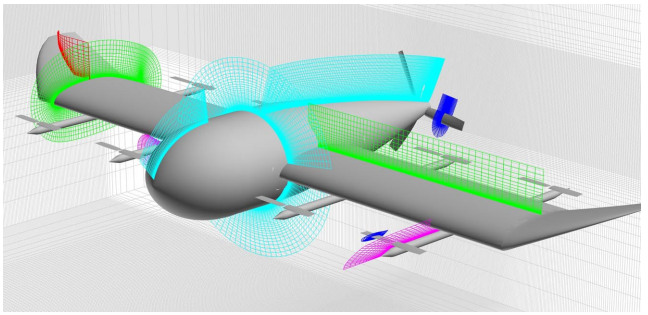

Fig. 2 Details of near-body and background grids.

flows at subsonic speeds. Typical resolution near surface is 10^{-4} of reference length such as chord of wings and blades.

III. Trajectory Equations

In this effort, it is assumed that all components undergo rigid body motions with or without rotations. The configuration is modeled to undergo vertical (y) and forward (x) motions and rotation about the center of mass.

T, L, D, and G are thrust of pushing propeller, lift from lifting propellers and wing–body, drag of full configuration, and gravitational forces in lbs. Angle of attack in degrees is represented by α. The equations of motions can be written as

$$m\ddot{x} = T\cos(\alpha) + L\sin(\alpha) - D\cos(\alpha) \tag{1a}$$

$$m\ddot{y} = T\sin(\alpha) + L\cos(\alpha) - D\sin(\alpha) - G \tag{1b}$$

where $G = mg$ (m is mass in slugs, and g is acceleration due to gravity in feet/s^2. L and D can be expressed as $1/2\rho V^2 S C_l$ and $1/2\rho V^2 S C_d$, where S is surface area, ρ is air density in slugs/ft^3, and V is velocity in feet/s. C_l and C_d are lift and drag force coefficients. Assuming a small angle of attack and defining the following:

$$\cos(\alpha) = \frac{\dot{x}}{\sqrt{\dot{x}^2 + \dot{y}^2}} = \frac{\dot{x}}{V}; \qquad \sin(\alpha) = \frac{\dot{y}}{\sqrt{\dot{x}^2 + \dot{y}^2}} = \frac{\dot{y}}{V}$$

Equations (1) can be written as

$$\begin{bmatrix} 1 & 0 \\ 0 & 1 \end{bmatrix} \begin{Bmatrix} \ddot{x} \\ \ddot{y} \end{Bmatrix} + p \begin{bmatrix} C_d & C_l \\ -C_l & C_d \end{bmatrix} \begin{Bmatrix} \dot{x} \\ \dot{y} \end{Bmatrix} = \begin{Bmatrix} 0 \\ -g \end{Bmatrix} + \frac{1}{m} \begin{Bmatrix} T \\ 0 \end{Bmatrix} \tag{2}$$

where $p = \rho V S/2m$.

Equation (2) is solved time accurately by using the Newmark Time Integration Scheme [15].

The aerodynamic quantities C_l, C_d, and T are computed by solving RANS equations with the OVERFLOW code and are used to solve Eq. (2) at every step. The rigid body motions from Eq. (2) are fed back to OVERFLOW codes using interface data files, as reported in Ref. [16].

IV. Validations with the Lifting Line Theory

Given the fast-evolving new configurations and proprietary restrictions, data for validation seldom exist for air taxis. This paper relies on the use of the well-validated code OVERFLOW [17], accepted engineering practices for grids [14], and validation with lifting line theory (LLT) based on the linear aerodynamics. Because the flows over rotating propeller blades play significant role in the trajectory motion, its aerodynamic responses are validated with LLT based on simplified linear aerodynamics assumptions [18].

Computations are made for isolated lifting and pushing propeller blades. The lifting propeller is forced to rotate at 4800 revolutions per minute (RPM), a speed required so that the LCAT reaches an altitude of 1500 feet with 15 feet/s final velocity assuming a total weight of 600 lbs. Figure 3 shows the responses of force coefficients that have reached a periodic state.

Figure 4 shows comparison of sectional force coefficient C_n between NS and LLT results. Both compare well in trend. The LLT results appear to overpredict forces, as compared with the NS results.

Similar comparisons are obtained for pushing blade rotating at 2800 RPM. A periodic response is obtained within 6 cycles, with a 0.25 deg rotation per step.

Figure 5 shows the Mach number and coefficient of pressure Cp distribution of the upper surface of the pushing propeller. The tip Mach number is 0.414, corresponding to 2800 RPM.

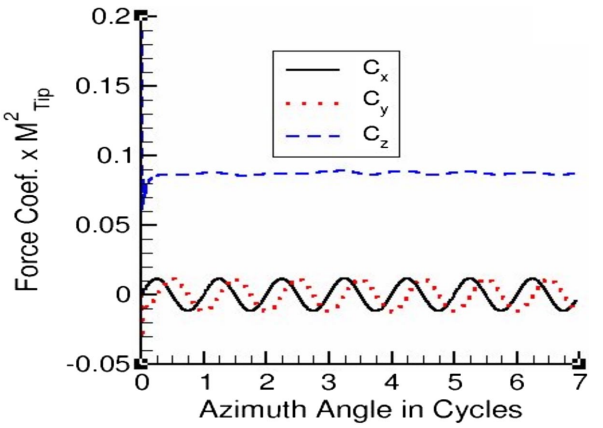

Fig. 3 Responses of total aerodynamic forces on lifting propeller blade.

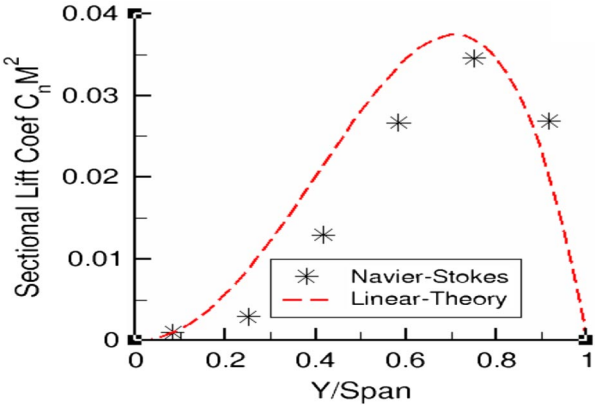

Fig. 4 Comparison of sectional lift forces along span for lifting propeller blade.

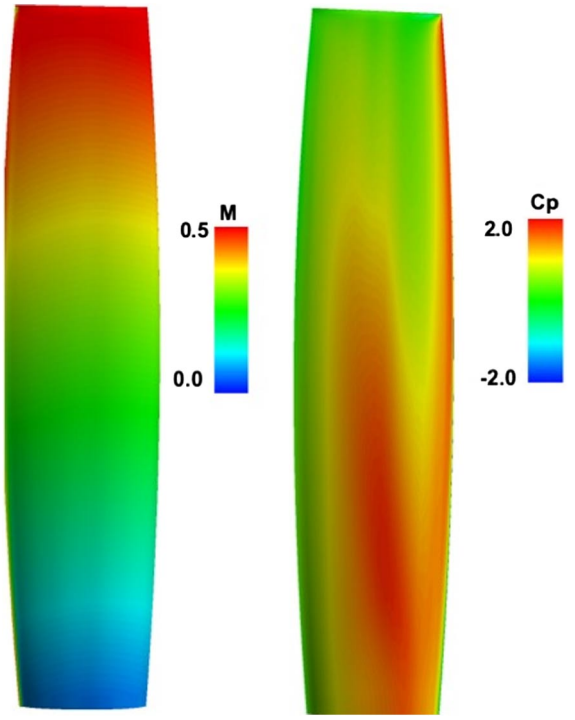

Fig. 5 Snapshot of upper surface Mach number and Cp distribution of the pushing propeller blade.

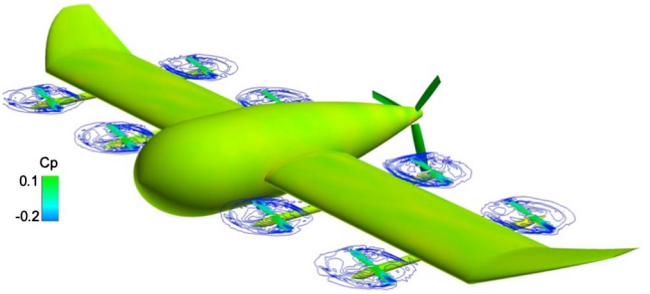

Fig. 7 Snapshots of the surface Cp and field Mach number distributions during vertical takeoff.

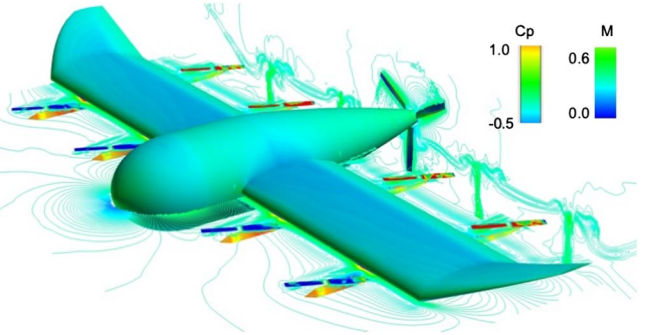

Fig. 8 Snapshot of surface Cp and field Mach number distributions during forward motion.

V. Trajectory Responses

Computations are made for the LCAT to simulate a takeoff trajectory. It is assumed that the wing chord length and total span are 2.5 and 32 feet, respectively, with a total weight of 600 lbs. The LCAT will reach an altitude of h feet, with vertical velocity of v feet/s, before forward motion takes place. The thrust needed by lifting propellers is given by $T = m(a + g)$, where acceleration $a = v^2/(2h)$, assuming an initial velocity of zero. Based on thrust computed on isolated blades, the lifting propeller blade needs to rotate at 4800 RPM so that the LCAT reaches an altitude of 1500 feet with 15 feet/s final vertical velocity.

The first computations are made at forward velocity $M_\infty = 0.20$, with nonrotating blades to check the convergence. Total lift and drag forces converged by 4 orders of magnitude with 4000 iterations. Fluctuations in drag force were more than those of lift force.

Computations are made for six cycles of LPB rotation, whereas the PPB is stationary with zero freestream Mach number. With the obtained initial conditions, integration of Eq. (2) is started. When an altitude of 1500 feet is reached, the RPM of LPB started reducing, and the rotation of PPB is started. The RPM of PPB is determined, assuming that the LCAT reaches a maximum freestream forward velocity of 200 feet/s in 1500 feet. Based on the thrust computed on the isolated PPB, and the drag of the LCAT configuration computed at $M_\infty = 0.20$, an RPM of 2800 is needed for the PPB. A plot of trajectory paths is shown in Fig. 6 for both vertical and forward motions.

A snap shot surface Cp and field Mach number contours are shown in Figs. 7 and 8 at the 5th second (in vertical motion) and 18th second (during forward motion). Because of low vertical acceleration, the Cp values are low for the wing–body configuration in Fig. 7.

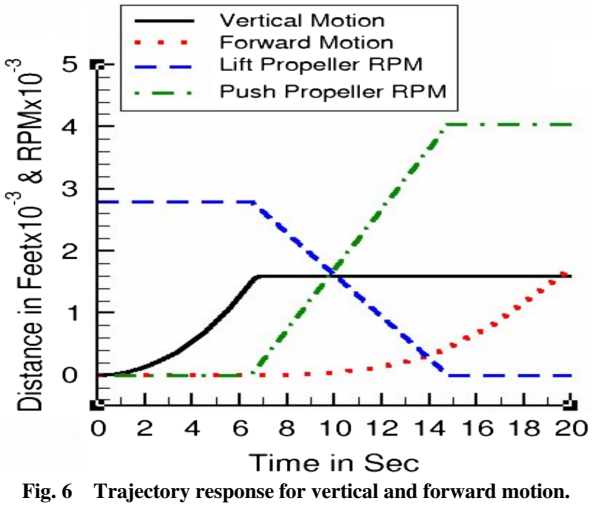

Fig. 6 Trajectory response for vertical and forward motion.

VI. Conclusions

A procedure to embed the trajectory equations of an LCAT in an overset-based RANS software primarily designed for rigid configurations is presented. Unsteady aerodynamic results from the present development compare well with lifting line theory results for isolated lifting and pushing propeller blades. This effort will provide a guideline for advanced stability computations using computational fluid dynamics for design of air taxis. Future work will involve extending the present time-accurate approach to simulate aeroelasticity of configurations with multiple propellers.

Acknowledgment

This work was supported by the NASA Advanced Supercomputing (NAS) Division under the activity of advancing computational fluid dynamics for real-world flight simulations of aerospace vehicles.

References

[1] "NASA's UAM Grand Challenge," https://www.nasa.gov/aero/nasa-completes-multi-drone-test-in-downtown-reno/ [retrieved 8 Jan. 2020].

[2] Hill, G. C., and Waters, M. H., "Conceptual Design of a Lift Fan Plus Lift/Cruise Fighter," *Journal of Aircraft*, Vol. 12, No. 10, Oct. 1975,

pp. 763–768.
https://doi.org/10.2514/3.59870
[3] Piñero, E., Jr., "The Year of Electric-Powered Lift," Aerospace America, Dec. 2018.
[4] Hyatt, K., "Kitty Hawk and Boeing are Teaming up on Flying Cars," CNET News, June 2019, https://www.cnet.com/roadshow/news/boeing-kitty-hawk-flying-car-partnership/ [retrieved 8 Jan. 2020].
[5] Bushnell, D. M., "Two Big Aerospace Ideas," Aerospace America, Sept. 2019, pp. 40–43.
[6] Ventura Diaz, P., Johnson, W., Ahmad, J., and Yoon, S., "The Side-by-Side Urban Air Taxi," *AIAA Aviation 2019 Forum*, AIAA Paper 2019-2828, June 2019.
https://doi.org/10.2514/6.2019-2828
[7] Peyret, R., and Viviand, H., "Computation of Viscous Compressible Flows Based on Navier–Stokes Equations," AGARD AG-212, 1975.
[8] Deere, K. A., Viken, J. K., Viken, S. A., and Carter, M. B., "Computational Analysis of a Wing Designed for the X-57 Distributed Electric Propulsion, Aircraft," *35th AIAA Applied Aerodynamics Conference*, AIAA Paper 2017-3923, 2017.
https://doi.org/10.2514/6.2017-3923
[9] Wood, D. H., "Full-Scale Tests of Metal Propellers at High Tip Speeds," NACA TR-375, 1929.
[10] Buing, P. G., and Pulliam, T. H., "Near-Body Grid Adaption for Overset Grids," *46th AIAA Fluid Dynamics Conference*, AIAA Paper 2016-3326, 2016.
https://doi.org/10.2514/6.2016-3326
[11] Spalart, P. R., "Direct Simulation of a Turbulent Boundary Layer," *Journal of Fluid Mechanics*, Vol. 187, Feb. 1988, pp. 61–98.
[12] Guruswamy, G. P., "Performance of the Widely-Used CFD Code OVERFLOW on the Pleaides Supercomputer," NASA TM-2017-219510, May 2017.
[13] Chan, W. M., "Overgrid Version 2.4," 2018, https://www.nas.nasa.gov/publications/software/docs/chimera/pages/overgrid.html
[14] Guruswamy, G. P., "Modeling of Oscillating Control Surfaces Using Overset-Grid-Based Navier–Stokes Equations Solver," *ASME Journal of Dynamic Systems, Measurement, and Control*, Vol. 139, No. 3, Jan. 2017, Paper DS-16-1010.
https://doi.org/10.1115/1.4034945
[15] Bathe, K. J., "Direct Integration Methods," *Finite Element Procedures*, Prentice-Hall, Englewood Cliffs, NJ, 1966, pp. 769–782.
[16] Guruswamy, G. P., "Dynamic Aeroelasticity of Wings with Tip Propeller by Using Navier–Stokes Equations," *AIAA Journal*, Vol. 57, No. 8, 2019, pp. 3200–3205.
https://doi.org/10.2514/1.J058610
[17] Guruswamy, G. P., "Time-accurate Aeroelastic Computations of a Full Helicopter Model Using the Navier–Stokes Equations," *International Journal of Aerospace Innovations*, Vol. 5, Nos. 3–4, Dec. 2013, pp. 73–82.
https://doi.org/10.1260/1757-2258.5.3-4.73
[18] Cantwell, B. J., *Fundamentals of Compressible Flow*, 2007, pp. 20–23, Chap. 12, https://www.scribd.com/document/363515543/AA210-Fundamentals-of-Compressible-Flow-Ch-14-BJ-Cantwell [retrieved 8 Jan. 2020].

P. Givi
Associate Editor